The Company of **Biologists**

RESEARCH ARTICLE

Novel phosphorylation states of the yeast spindle pole body

Kimberly K. Fong[1,*], Alex Zelter[1], Beth Graczyk[1,‡], Jill M. Hoyt[1], Michael Riffle[1], Richard Johnson[2], Michael J. MacCoss[2] and Trisha N. Davis[1,§]

ABSTRACT

Phosphorylation regulates yeast spindle pole body (SPB) duplication and separation and likely regulates microtubule nucleation. We report a phosphoproteomic analysis using tandem mass spectrometry of enriched *Saccharomyces cerevisiae* SPBs for two cell cycle arrests, G1/S and the mitotic checkpoint, expanding on previously reported phosphoproteomic data sets. We present a novel phosphoproteomic state of SPBs arrested in G1/S by a *cdc4-1* temperature-sensitive mutation, with particular focus on phosphorylation events on the γ-tubulin small complex (γ-TuSC). The *cdc4-1* arrest is the earliest arrest at which microtubule nucleation has occurred at the newly duplicated SPB. Several novel phosphorylation sites were identified in G1/S and during mitosis on the microtubule nucleating γ-TuSC. These sites were analyzed *in vivo* by fluorescence microscopy and were shown to be required for proper regulation of spindle length. Additionally, *in vivo* analysis of two mitotic sites in Spc97 found that phosphorylation of at least one of these sites is required for progression through the cell cycle. This phosphoproteomic data set not only broadens the scope of the phosphoproteome of SPBs, it also identifies several γ-TuSC phosphorylation sites that influence microtubule formation.

INTRODUCTION

The centrosome is the microtubule organizing center of the cell, responsible for nucleating microtubules and establishing a bipolar spindle during mitosis. In budding yeast, the spindle pole body (SPB) is the functional equivalent of the centrosome in higher eukaryotic cells and the essential yeast spindle pole components have homologues in humans (Flory and Davis, 2003; Jaspersen and Winey, 2004; Lin et al., 2014; Oakley et al., 1990; Stearns et al., 1991). However, the yeast SPB exhibits a morphologically distinct structure from higher eukaryotic centrosomes. In contrast to the fluid matrix of the pericentriolar material built around the centrioles of mammalian centrosomes (Woodruff et al., 2014, 2015), the SPB exists as three highly organized,

stratified layers built around a crystalline core of Spc42 (Bullitt et al., 1997; Byers and Goetsch, 1975; O'Toole et al., 1999; Viswanath et al., 2017). Our understanding of SPB structure and composition has been advantageously used to understand highly conserved mechanisms of centrosomal regulation through phosphorylation (Bouhlel et al., 2015; Jaspersen et al., 2004; Winey et al., 1991). Centrosomes serve as signaling platforms, integrating cell signals to regulate the localization of spindle proteins and progression through the cell cycle (Basto and Pines, 2007; Burns et al., 2015; Casenghi et al., 2005; Cha et al., 2004; Jaspersen and Winey, 2004; Jiang et al., 2006; Lange, 2002; Rieder et al., 2001; Winey and Bloom, 2012). More specifically, kinases Mps1, Polo, Hrr25, and Cdk1 have been implicated in the regulation of SPB duplication, SPB separation, and cell cycle transitions (Avena et al., 2014; Castillo et al., 2002; Deshaies and Ferrell, 2001; Jaspersen and Winey, 2004; Jaspersen et al., 2004; Peng et al., 2015; Winey et al., 1991).

Previous research shows that all SPB proteins are phosphoproteins. Two of the best characterized phosphoproteins at the SPB are Tub4 and Spc110, both implicated in microtubule nucleation. Several individual phosphorylation sites have been identified and mutated in Tub4. Phosphomimetic mutations of highly conserved Tub4 sites induce a mitotic arrest and confer defects in spindle assembly (S360) (Keck et al., 2011; Lin et al., 2011), increase microtubule assembly rates and numbers of microtubules at the SPB (Y445) (Vogel et al., 2001), and induce metaphase arrests with short, disorganized spindles (S74 and S100) (Lin et al., 2011). Likewise, Spc110 phosphorylation has been studied extensively *in vivo* (Friedman et al., 1996, 2001; Huisman et al., 2007; Stirling and Stark, 1996). Mps1 phosphorylation of Spc110 S60, T64, and T68 is responsible for a gel shift during mitosis (Friedman et al., 1996, 2001; Stirling and Stark, 1996) and blocking phosphorylation of S91 induces a metaphase delay (Huisman et al., 2007). A compilation of previously studied spindle pole component phosphorylation sites can be found in the Supplementary Data S1.

Two large-scale analyses of SPB phosphorylation have been performed. Valuable identification of phosphorylation sites in the γ-tubulin small complex (γ-TuSC) relied on material overexpressed in yeast, which could alter the phosphorylation pattern (Lin et al., 2011). Phosphoanalysis of enriched SPBs identified 298 sites but sequence coverage of the γ-TuSC was poor compared to the coverage of the other components (Keck et al., 2011).

Using our improved SPB enrichment protocol (Fong et al., 2016) and relying on advances in mass spectrometers and analysis packages, we have conducted a new phosphoanalysis of isolated SPBs. Our data expand on previously reported phosphoproteomic data sets and identify novel cell cycle phosphorylation states of the SPB at the onset of microtubule nucleation in G1/S, a cell cycle stage not previously examined. Our phosphorylation data of the microtubule nucleating γ-TuSC builds on the current literature by identifying and fluorescently analyzing new cell cycle phosphorylation sites of the specific population of γ-TuSCs attached to SPBs.

[1]Department of Biochemistry, University of Washington, Seattle, WA 98195, USA. [2]Department of Genome Sciences, University of Washington, Seattle, WA 98195, USA.
*Present address: Department of Physiology and Biophysics, University of Washington, Seattle, WA 98195, USA. ‡Present address: Laboratory of Biochemical Genetics and Metabolism, The Rockefeller University, New York, NY 10065, USA.

§Author for correspondence (tdavis@uw.edu)

T.N.D., 0000-0003-4797-3152

RESULTS AND DISCUSSION

Enrichment by TAP-tagged Spc97 increases the yield of intact spindle pole bodies

Previous studies have shown that SPBs from *Saccharomyces cerevisiae* co-purify with Mlp2, a nuclear pore component (Niepel et al., 2005). To increase the yield of isolated SPBs, tandem affinity purification (TAP) tags were introduced on spindle pole components (List of strains in Table 1). Starting with the proteins found in the core of the SPB, we tagged Spc42 and Cnm67. While N-terminally tagged Cnm67 was viable, we found that the core spindle pole component Spc42 tagged with a C-terminal TAP tag was not viable in our strain background. In addition to core proteins, we tagged membrane anchor proteins Nbp1 and Bbp1, linker proteins Spc110 and Spc72, and γ-TuSC component Spc97 with C-terminal TAP tags.

We used western blot analysis to assess the yield of enriched SPBs and found that Mlp2-TAP bound weakly to IgG beads, resulting in a low yield of enriched SPBs. Similarly, Bbp1-TAP, Nbp1-TAP and Spc72-TAP showed weak or no binding to IgG beads. Other constructs (TAP-Cnm67 and Spc110-TAP) showed relatively strong binding to IgG beads, but TEV (tobacco etch virus) protease cleavage failed to remove the bound SPBs from the beads, again resulting in low yields. A C-terminal TAP tag on Spc97 was shown not only to bind the strongest to IgG beads, but to be efficiently cleaved from the beads by TEV protease, resulting in the highest, most reproducible yield of enriched SPBs (Fig. 1A).

Spc97 is a component of the γ-TuSC, a stable heterotetrameric complex that exists free in solution as well as bound to the SPB.

Because our enrichment protocol relied on a TAP tag on Spc97, our protocol yielded free γ-TuSCs in addition to intact SPBs. Separation of intact SPBs and γ-TuSCs was achieved by velocity sedimentation (Fong et al., 2016). Analysis by western blot confirmed that SPBs were concentrated in fractions 9–11 of the sucrose gradient (40–50% sucrose) while the soluble fraction of the γ-TuSCs remained higher in the gradient (Fong et al., 2016).

Enriched spindle pole bodies are the same size as spindle pole bodies *in vivo*

To determine if enriched SPBs were intact and the same size as *in vivo*, SPBs were isolated from strains that contained either Spc42-GFP or Tub4-GFP. Quantification of the fluorescence intensities verified enriched SPBs containing Spc42-GFP had the same fluorescence intensity as Spc42-GFP SPBs in live cells, suggesting that the core of the SPB remained intact through the enrichment protocol. To test if the inner and outer plaques were retained during the enrichment protocol, SPBs containing Tub4-GFP were isolated and imaged *in vitro* and *in vivo*. Quantification of fluorescence intensity indicated that isolated SPBs retained 88% of the γ-TuSC compared to SPBS in live cells (Fig. 1B). Finally, all 18 proteins were present as determined by high protein coverage in mass spectrometry (Table 2).

Tandem mass spectrometry data identified phosphorylation sites of the spindle pole body at different cell cycle stages

SPBs were enriched from different stages of the cell cycle to identify cell cycle specific phosphorylation events. The phosphorylation

Table 1. Strains used in this study

Strain	Genotype	Reference
W303	*ade2-1oc can1-100 his3-11, 15 leu2-3,112 trp1-1 ura3-1*	
LAY57-1B	*MATα SPC110-TAP::kanMX*	This study
BGY64-1B	*MATa SPC72-TAP::kanMX*	This study
BGY68-16A	*MATa SPC42-GFP::kanMX SPC97-TAP::kanMX*	This study
BGY69-1B	*MATα NBP1-TAP::kanMX*	This study
BGY70-2B	*MATa BBP1-TAP::kanMX*	This study
BGY72-8A	*MATa SPC42-mCherry::hphMX SPC97-TAP::kanMX*	Fong et al., 2016
BGY74-17B	*MATα SPC42-mCherry::hphMX SPC97-TAP::kanMX TUB4-GFP::kanMX*	Fong et al., 2016
TAP-CNM67	*MATa TAP-CNM67::kanMX*	This study
SPC97-TAP	*MATa SPC97-TAP::kanMX*	This study
KFY37-4C	*MATa ade3Δ-100 LEU2::GFP-TUB1 lys2Δ::HIS3 SPC42-mCherry::hphMX spc98Δ::kanMX pKF12*	This study
KFY38-5C	*MATa ade3Δ-100 LEU2::GFP-TUB1 lys2Δ::HIS3 SPC42-mCherry::hphMX spc97Δ::TRP1 pTN25*	This study
KFY194	*MATa ade3Δ-100 LEU2::GFP-TUB1 lys2Δ::HIS3 SPC42-mCherry::hphMX spc97(S208A/S209A)::URA3 spc97Δ::TRP1 pTN25*	This study
KFY196	*MATa ade3Δ-100 LEU2::GFP-TUB1 lys2Δ::HIS3 SPC42-mCherry::hphMX spc97(S208D/S209D)::URA3 spc97Δ::TRP1*	This study
KFY220-4B	*MATa ade3Δ-100 LEU2::GFP-TUB1 lys2Δ::HIS3 SPC42-mCherry::hphMX tub4Δ::kanMX pLA11*	This study
KFY229	*MATa ade3Δ-100 LEU2::GFP-TUB1 lys2Δ::HIS3 SPC42-mCherry::hphMX spc97(S208A)::URA3 spc97Δ::TRP1*	This study
KFY230	*MATa ade3Δ-100 LEU2::GFP-TUB1 lys2Δ::HIS3 SPC42-mCherry::hphMX spc97(S209A)::URA3 spc97Δ::TRP1*	This study
KFY313-33D	*MATa CDC20-AID::kanMX PDS1-myc18::LEU2 ura3::pADH1-OsTIR1-9myc::URA3 SPC42-mCherry::hphMX SPC97-TAP::kanMX*	This study
KFY332-12C	*MATa cdc4-1 SPC42-mCherry::hphMX SPC97-TAP::kanMX*	This study
KFY338	*MATa ade3Δ-100 LEU2::GFP-TUB1 lys2Δ::HIS3 SPC42-mCherry::hphMX spc97(S84A)::URA3 spc97Δ::TRP1*	This study
KFY339	*MATa ade3Δ-100 LEU2::GFP-TUB1 lys2Δ::HIS3 SPC42-mCherry::hphMX spc97(S84D)::URA3 spc97Δ::TRP1*	This study
KFY340	*MATa ade3Δ-100 LEU2::GFP-TUB1 lys2Δ::HIS3 SPC42-mCherry::hphMX spc97(T88A)::URA3 spc97Δ::TRP1*	This study
KFY341	*MATa ade3Δ-100 LEU2::GFP-TUB1 lys2Δ::HIS3 SPC42-mCherry::hphMX spc97(T88D)::URA3 spc97Δ::TRP1*	This study
KFY342	*MATa ade3Δ-100 LEU2::GFP-TUB1 lys2Δ::HIS3 SPC42-mCherry::hphMX spc97(S84A/T88A)::URA3 spc97Δ::TRP1*	This study
KFY343	*MATa ade3Δ-100 LEU2::GFP-TUB1 lys2Δ::HIS3 SPC42-mCherry::hphMX spc97(S84D/T88D)::URA3 spc97Δ::TRP1*	This study
KFY352	*MATa ade3Δ-100 LEU2::GFP-TUB1 lys2Δ::HIS3 SPC42-mCherry::hphMX spc97(S797A)::URA3 spc97Δ::TRP1*	This study
KFY353	*MATa ade3Δ-100 LEU2::GFP-TUB1 lys2Δ::HIS3 SPC42-mCherry::hphMX spc97(S797D)::URA3 spc97Δ::TRP1*	This study
KFY356	*MATa ade3Δ-100 LEU2::GFP-TUB1 lys2Δ::HIS3 SPC42-mCherry::hphMX spc98(S152A)::URA3 spc98Δ::kanMX*	This study
KFY357	*MATa ade3Δ-100 LEU2::GFP-TUB1 lys2Δ::HIS3 SPC42-mCherry::hphMX spc98(S152D)::URA3 spc98Δ::kanMX*	This study
KFY358	*MATa ade3Δ-100 LEU2::GFP-TUB1 lys2Δ::HIS3 SPC42-mCherry::hphMX tub4(S71A)::URA3 tub4Δ::kanMX*	This study
KFY359	*MATa ade3Δ-100 LEU2::GFP-TUB1 lys2Δ::HIS3 SPC42-mCherry::hphMX tub4(S71D)::URA3 tub4Δ::kanMX*	This study
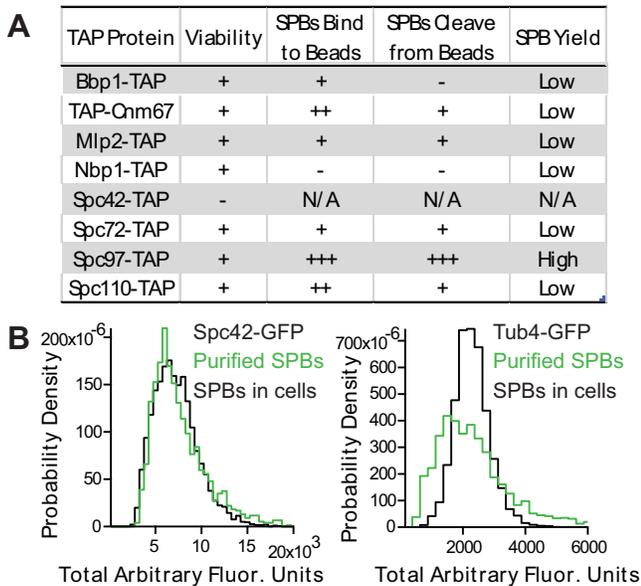
Fig. 1. Enrichment protocol yields intact spindle pole bodies.
(A) Several components of the spindle pole body (SPB) were tagged with a TAP tag. SPBs were isolated using each tag and the yield of SPBs determined. The efficiency of SPBs binding to beads and being cleaved from beads were determined by western blot analysis. (B) Enriched SPBs are the same size as SPBs in cells, as determined by fluorescence intensities of SPBs containing either Spc42-GFP or Tub4-GFP imaged in cells (in black) and after enrichment (in green).

state of SPBs at G1/S had not been previously described. We isolated SPBs from *cdc4-1* cells, which were arrested in G1/S by a shift to the restrictive temperature of 36°C. To identify the subset of phosphorylation sites present during mitosis, SPBs were harvested from cells arrested in mitosis by depletion of Cdc20. Finally, we isolated SPBs from asynchronous cultures. Western blot analysis

Table 2. Sequence coverage (%) of SPB proteins by mass spectrometry

	Asynchronous SPBs			Mitotic SPBs Cdc20-AID			G1/S SPBs cdc4-1	
Bbp1	67	52	0	41	18	64	78	70
Cdc31	71	52	44	52	47	68	72	74
Cmd1	63	50	33	50	47	88	63	63
Cnm67	71	57	46	55	71	85	74	69
Kar1	63	40	0	29	29	47	69	61
Mps2	49	39	0	31	7	37	69	59
Mps3	49	29	2	24	20	60	59	51
Nbp1	53	40	0	32	21	50	53	52
Ndc1	35	20	0	17	19	39	55	38
Nud1	49	36	28	28	62	59	75	57
Sfi1	41	23	0	15	7	24	40	31
Spc29	76	49	14	60	69	71	76	68
Spc42	77	52	27	56	69	80	82	79
Spc72	58	40	42	32	67	69	69	61
Spc97	52	41	45	35	73	65	72	62
Spc98	42	35	29	29	52	58	61	49
Spc110	69	58	31	54	57	69	75	72
Tub4	46	10	20	21	62	61	68	52

Each column corresponds to a biological replicate. For each biological replicate, with the exception of the first asynchronous SPB sample, two technical replicates were individually analyzed by Comet (Eng et al., 2013), then combined for Percolator (Käll et al., 2007) and protein inference analyses. Three biological replicates were completed for asynchronous SPBs, three for mitotic SPBs, and two for G1/S SPBs. The percentage sequence coverage for each SPB protein is shown.

after velocity sedimentation verified the presence of SPBs in fractions 9–11 of the sucrose gradient (40–50% sucrose) using antibodies against Spc110 and Spc97 (Fig. 2A).

Phosphorylation sites were identified by mass spectrometry and verified manually to eliminate any ambiguous or unsubstantiated assignments. For the phosphoproteomic data set reported here, 212 phosphorylation sites were reported across asynchronous, mitotic, and G1/S SPBs (Fig. 2B; Supplementary Data S1). Of the sites reported in this study, 60 (28%) were only identified in mitotic SPBs, and 24 (11%) were only identified in G1/S SPBs and 26 (12%) were only detected in the asynchronous SPB sample. Forty-three sites (20%) were found in SPBs from all three conditions.

A previous study of the yeast SPB phosphoproteome reported 298 phosphorylation sites in the 18 SPB components throughout the cell cycle (Keck et al., 2011). However, since publication, advances in the resolution and sensitivity of mass spectrometers and new software packages that apply stringent quality cutoffs increased the confidence in phosphorylation assignments. Of the phosphorylation sites identified in this current study, 113 phosphorylation sites were also identified in Keck et al. (2011), resulting in 28% (113/397 total sites) of all detected sites appearing in both data sets. To determine if the difference between the data sets was due to how the mass spectra were analyzed, we reanalyzed the raw data from Keck et al. (2011) using Comet and Percolator, the same algorithms used for our new data set. The reanalysis of the Keck et al. (2011) raw data set resulted in a reduction from 298 published phosphorylation sites to 168 phosphorylation sites [for more about statistical analysis, phosphorylation assignments, reanalysis of Keck et al. (2011) data, and dataset comparisons, see Table S1 and Figs S1–S12]. Many ambiguous assignments were removed from the previously published data set by imposing strict statistical cutoffs for spectra included in the data set. The reanalysis of previously published data and our new data set showed 42% (112/268 total sites) agreement (Fig. 2C, Supplementary Data S1). The 56 sites identified in the reanalyzed published data, but not this data set, most likely result from the fact that the Keck et al. (2011) sample was enriched for phosphopeptides by running the sample over a titanium dioxide column (Keck et al., 2011). In contrast, phosphopeptides were not enriched for this data set, thus some rare phosphorylation events were likely missed. The 100 sites only identified in this study might result from improved SPB enrichment protocols or advances in mass spectrometer instrumentation and sensitivity.

Previous work focused on phosphorylation of the γ-TuSC overexpressed and purified from yeast (Lin et al., 2011). Looking at the γ-TuSC phosphorylation sites in Spc97, Spc98, and Tub4 identified in our data set, we find that 15 of the sites agreed with the reported literature. However, our data has identified 11 additional sites, six of which were identified in G1/S SPBs, on γ-TuSC that might inform our understanding of the phosphorylation state specifically when attached to the SPB (Fig. 2D).

The phosphorylation profile of G1/S spindle pole bodies include sites present at the initiation of microtubule nucleation

Previous studies on SPB phosphorylation used alpha factor to arrest the cells in G1 (Keck et al., 2011). We report a novel phosphorylation state of SPBs from cells arrested in G1/S with a *cdc4-1* temperature sensitive arrest. These two G1 arrests differ in the state of the SPB and in the active cyclins present. In an alpha factor arrest, the SPBs are not duplicated and Cln-Cdk1 is inhibited (Gartner et al., 1998; Jeoung et al., 1998; Peter and Herskowitz, 1994). In contrast, in a *cdc4-1* temperature sensitive arrest, the SPBs
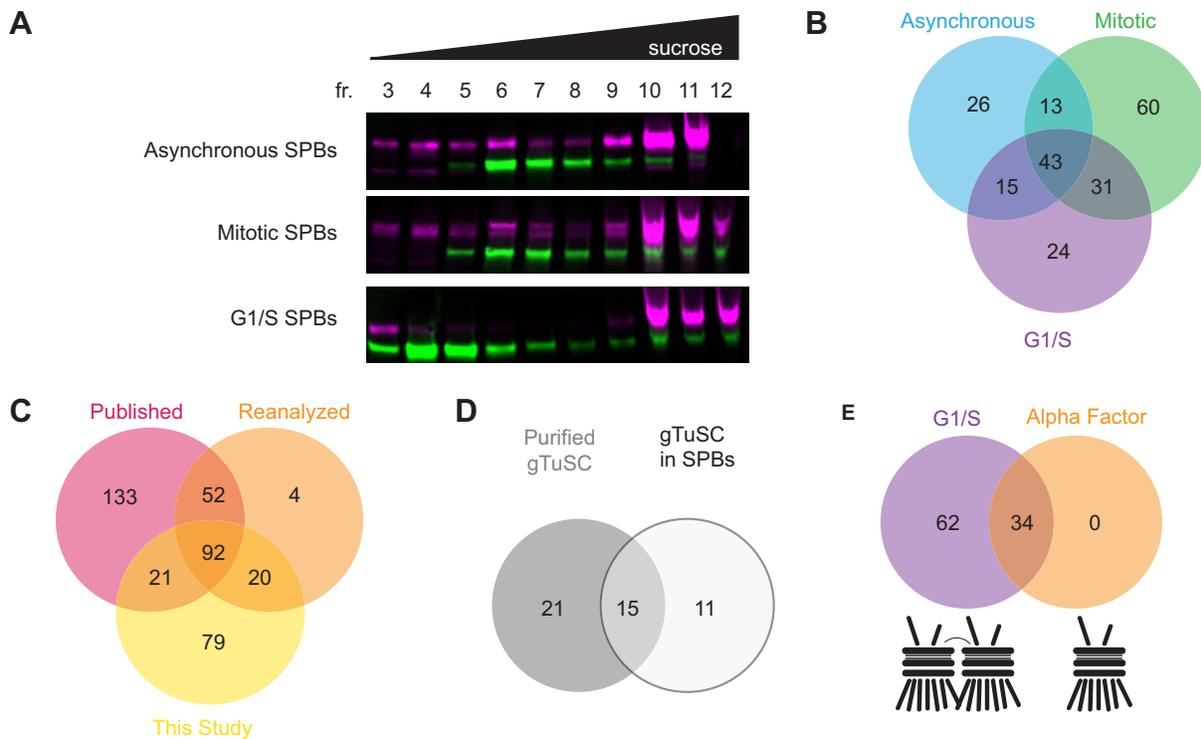
Fig. 2. Comparison of phosphoproteomic data sets for the spindle pole body isolated from different cell cycle stages. (A) Asynchronous, mitotic, and G1/S SPBs were isolated. Fractions containing intact SPBs were determined by western blot analysis, using antibodies against Spc110 (in magenta) and Spc97 (in green). Sucrose concentration increases from left to right. Fractions with high concentrations of spindle pole bodies (Fractions 9, 10, 11 for asynchronous SPBs; Fractions 10, 11, for mitotic SPBs and G1/S SPBs) were used for phosphoproteomic mass spectrometry analysis. (B) Comparison of high resolution phosphoproteomic data collected in this study for asynchronous wild-type (in blue), mitotic (in green), and G1/S (in purple) SPBs. (C) Comparison of the phosphoproteome published in Keck et al. (2011) (in red), reanalysis of Keck et al. (2011) data (in orange), and data collected in this study (in yellow). (D) Comparison of γ-tubulin small complex phosphorylation sites identified in overexpressed γ-tubulin subcomplexes [Lin et al. (2011); in grey] and identified in the context of the intact SPB (this study; in white). (E) Comparison of G1 SPBs arrested by *cdc4-1* or alpha factor. In *cdc4-1* arrest, as indicated by the cartoon, the SPBs are duplicated, but not separated and both the new and the old SPBs are nucleating microtubules. In an alpha factor arrest, the SPB has not yet duplicated.

are duplicated but not separated (Byers and Goetsch, 1974; Pereira et al., 1998) and there are high levels of Cln-Cdk1 and low activity of Clb-Cdk1 (Blondel et al., 2000; Duncker et al., 1999). The *cdc4-1* shift to the restrictive temperature results in the earliest cell cycle arrest in which the newly duplicated SPB has nucleated microtubules, suggesting that the phosphorylation profile at this arrest is the earliest state conducive to high microtubule nucleation activity. Interestingly, all phosphorylation events detected during an alpha factor arrest were also identified in a G1/S arrest. However, there were several additional G1/S phosphorylation events that were detected in SPBs at this stage of the cell cycle (Fig. 2E).

In alpha-factor arrested SPBs from Keck et al. (2011), very few phosphorylation sites were identified on the γ-TuSC (Spc97, Spc98 and Tub4) or the proteins that bind the γ-TuSC to the core of the SPB (Spc72 and Spc110) (Keck et al., 2011). In fact, reanalysis of the published data failed to identify any unique G1 phosphorylation events for any of these five proteins. In contrast, in this study each of the three γ-TuSC proteins – Spc97, Spc98, and Tub4 – contained phosphorylation sites only observed in G1/S SPBs as well as five G1/S phosphorylation sites on Spc110 (Supplementary Data S1).

Phosphorylation of the γ-tubulin small complex is required for establishment of a proper mitotic spindle length

We examined the role of γ-TuSC phosphorylation events on spindle morphology, focusing on sites predicted to interfere with interaction with Spc110. Spc97 S84 was identified in mitotic and G1/S SPBs

and T88 was identified as a phosphorylation event in G1/S. Both of these sites were identified in free γ-TuSC, but not in previous phospho-analyses of intact SPBs (Keck et al., 2011; Lin et al., 2011). These two sites map to the outer face of γ-TuSC, in a region predicted to interact with Spc110 (Fig. 3A). Phosphomimetic and phosphoblocking mutations of these sites were integrated into yeast strains with Spc42-mCherry to label the SPBs and GFP-Tub1 to label the microtubules (list of strains in Table 1; list of plasmids in Table 3). Spindle morphology and cell growth were determined by several metrics. The distribution of tubulin fluorescence was measured across spindles of varying lengths. In wild-type cells, the tubulin fluorescence clusters in a distinct peak on either side of the spindle midzone, correlating with the kinetochore microtubules. A wider distribution of tubulin fluorescence across the half-spindle and an increase of the fraction of tubulin fluorescence at the spindle midzone indicates misregulation of microtubule length distribution (Gardner et al., 2008). Spc97 S84A, Spc97 S84D, Spc97 T88A, and Spc97 T88D had little effect on tubulin fluorescence at the spindle midzone individually or in combinations, Spc97 S84A/T88A and Spc97 S84D/T88D (Fig. 3C–E, Table 4). Another determinant of spindle morphology is the distribution of spindle lengths. The mean spindle length ±s.d. was determined for each mutation using bootstrap analysis, then compared to the mean of wild-type cells (see the Materials and Methods section). Spc97 S84A and Spc97 S84D had little effect on the distribution of spindle lengths. Mutation of Spc97 T88, either phosphoblocking or phosphomimicking, showed a
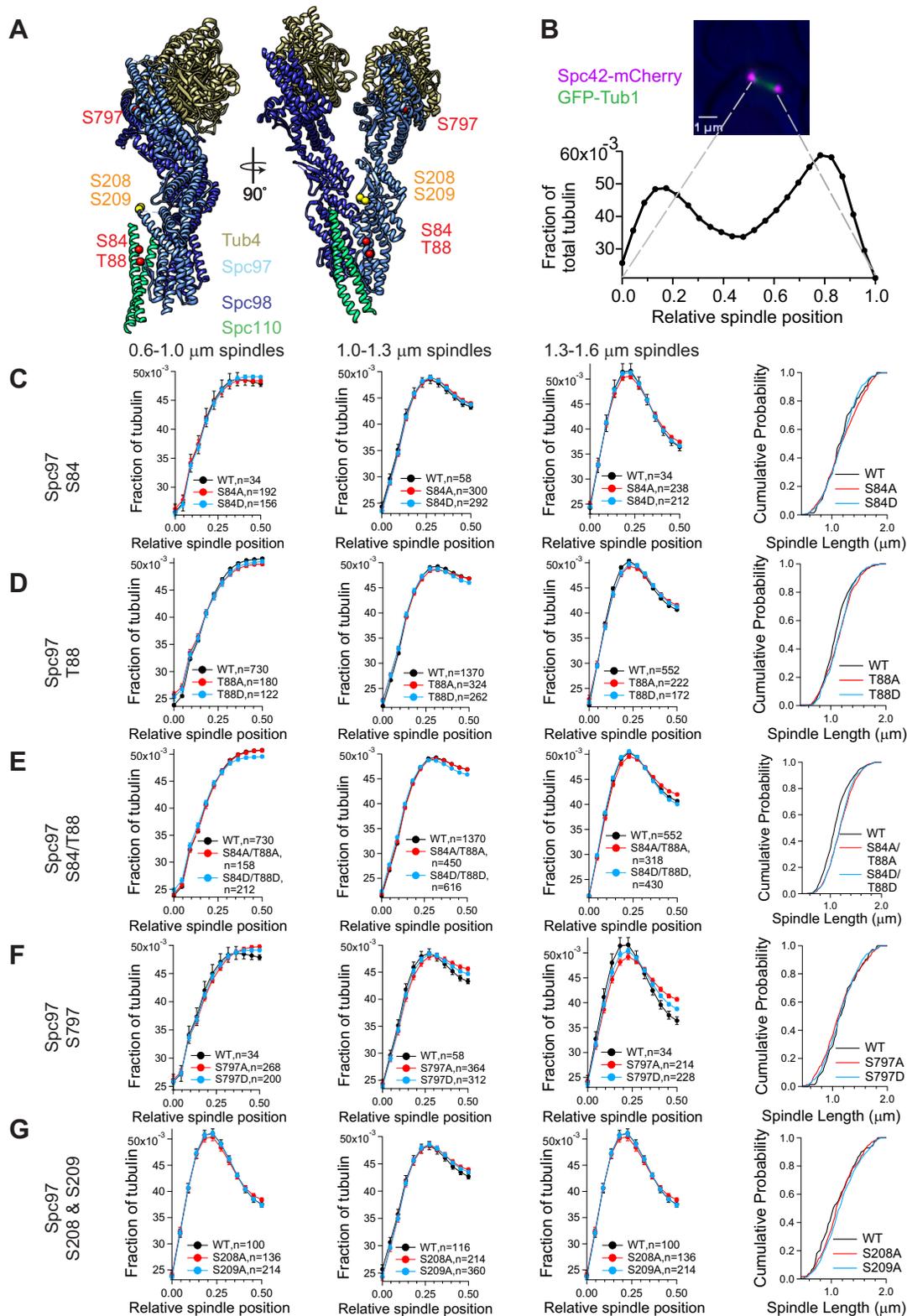
Fig. 3. See next page for legend.

statistically significant increase in spindle length distribution. The alleles carrying two mutations (S84A/T88A and S84D/T88D) both showed a further increase in spindle length (Fig. 3C–E, Table 4). And finally, cell growth was measured by budding index and comparison of large budded cell percentages. The individual mutations had little

effect on the percent of large budded cells, but S84A/T88A and S84D/T88D showed a slight increase in large budded cells, suggesting a delay in the cell cycle.

Similar analysis was conducted for Spc97 S797. Spc97 S797 was a novel phosphorylation site identified in mitotic SPBs and maps to the

Fig. 3. Phosphorylation of Spc97 is required for normal mitotic spindle morphology. (A) Mitotic and G1/S phosphorylation sites (in red) have been mapped onto the pseudo-atomic structure of Spc97 (light blue) in the yeast γ-tubulin small complex, adapted from PDB:5FM1 (Greenberg et al., 2016). Phosphoblocking mutations of Spc97 S208 and S209 (in yellow) in combination are lethal. (B) Spindle morphology was determined by measuring spindle length and tubulin fluorescence distribution along the spindle. Metaphase spindles were identified as spindles with 1.3–1.6 µm between Spc42-mCherry spindle poles. GFP-Tub1 fluorescence was measured across the entire spindle. (C–G) Half-spindle tubulin distribution profiles for spindles of a given length are shown for several Spc97 phosphorylation mutants. Spindle tubulin distributions were separated into two half spindles for ease of display (mean±s.e.m.). In each of the tubulin distribution graphs, the SPB is located at 0 and the spindle equator is located at 0.5. The far right panels show a cumulative probability of spindle length for the observed spindles, measured as the distance between Spc42-mCherry foci. Note that the x-axis begins at 0.45 µm to more clearly display the differences between traces.

C-terminal outer face of the γ-TuSC, which could also interact with Spc110 (Fig. 3A). While phosphomimicking and phosphoblocking mutations had no effect on spindle length, tubulin distribution was affected by these mutations, with an increase of tubulin at the spindle midzone, suggestive of misregulation of kinetochore microtubule length (Fig. 3F, Table 4).

Fluorescent spindle analysis was also performed for a G1/S site detected in Spc98 (S152) and a G1/S site detected in Tub4 (S71) (list of strains in Table 1; list of plasmids in Table 3). Spc98 S152 is a possible Cdk1 phosphorylation site, which was also observed in free γ-TuSC (Lin et al., 2011). While fluorescence analysis revealed no change in tubulin distribution across spindles of any length, the phosphomimetic mutation S152D showed a cell cycle delay with a statistically significant increase in the length of arrested spindles and an increase in large budded cells from 5.0% to 17.3% suggesting a checkpoint delay (Fig. 4C, Table 4). The novel G1/S phosphorylation site in Tub4 S71 sits at the interface between γ-tubulin and α-tubulin (Fig. 4A). The phosphoblocking mutation S71A resulted in longer spindles at the arrest and a cell cycle delay, with 18.3% large budded cells compared to 5.0% in wild-type cells (Fig. 4D). Phosphomimicking mutation of S71 also showed a cell cycle delay, with 27.7% large budded cells compared to 5.0% in wild-type cells; however, there was no change in spindle length distributions (Table 4).

We also examined sites identified in mitotic SPBs, hypothesizing that these sites could be involved in regulation of microtubules during the establishment of the mitotic spindle. In previously published phosphoproteomic data, γ-TuSC component Spc97 was found to have two phosphorylation sites unique to mitosis, S208 and S209 (Keck et al., 2011). Phosphomimetic mutations and phosphoblocking mutations were made for both mitotic phosphorylation sites and transformed into yeast (list of strains in Table 1; list of plasmids in Table 3). Using a plasmid shuffle assay, we determined that phosphomimicking mutations in Spc97 (S208D/S209D) were viable. However, the phosphoblocking mutations in Spc97 (S208A/S209A) were lethal. Spc97 S208A or Spc97 S209A were viable individually, with normal growth rates, morphologically wild-type spindles and wild-type tubulin distributions across metaphase spindles, suggesting that phosphorylation of at least one of these sites is required for progression through the cell cycle (Fig. 3G, Table 4). The locations of the Spc97 mitotic phosphorylation sites suggest that this region might be involved in interactions with Spc110. Disruption of the interface between Spc97 and Spc110 might destabilize the interaction between the γ-tubulin ring and Spc110.

Table 3. Plasmids used in this study

Plasmid	Relevant markers	Reference
pRS316	*CEN6 ARSH4 URA3 Amp^r f1 origin*	Sikorski and Hieter, 1989
pRS306	*URA3 f1 origin*	Sikorski and Hieter, 1989
pLA11	*TUB4 ADE3 LYS2 2µm origin*	This study
pKF12	*SPC98 ADE3 LYS2 2µm origin*	This study
pKF56	*SPC97 in pRS316*	This study
pKF137	*spc97(S208A/S209A) in pRS306*	This study
pKF161	*spc97(S208D/S209D) in pRS316*	This study
pKF191	*spc97(S208A) in pRS306*	This study
pKF192	*spc97(S209A) in pRS306*	This study
pKF244	*spc97(S84A) in pRS306*	This study
pKF245	*spc97(S84D) in pRS306*	This study
pKF246	*spc97(T88A) in pRS306*	This study
pKF247	*spc97(T88D) in pRS306*	This study
pKF248	*spc97(S84A/T88A) in pRS306*	This study
pKF249	*spc97(S84D/T88D) in pRS306*	This study
pKF258	*spc97(S797A) in pRS306*	This study
pKF259	*spc97(S797D) in pRS306*	This study
pKF262	*spc98(S152A) in pRS306*	This study
pKF263	*spc98(S152D) in pRS306*	This study
pKF264	*tub4(S71A) in pRS306*	This study
pKF265	*tub4(S71D) in pRS306*	This study
pSB2065	*3V5-IAA7-kanMX Amp^r f1 origin*	Gift from Sue Biggins*
pTN25	*SPC97 ADE3 2µm origin*	This study
PaTEVCa	*N-terminal TAP tag*	This study

*Fred Hutch Cancer Resource Center, Seattle, USA.

Conclusions

In summary, we optimized enrichment protocols to yield intact SPBs in quantities that facilitated *in vitro* analysis of SPB phosphorylation states by high-resolution mass spectrometry. While expanding on previously reported phosphorylation data sets, we were specifically interested in identifying phosphorylation sites in the γ-TuSC present at the SPB during G1/S arrest. We posit that that these G1/S sites reveal phospho-regulatory events important for the initiation of microtubule nucleation at the newly duplicated SPB. *In vivo*, mutation of G1/S and mitotic phosphorylation sites in the γ-TuSC illustrated the sensitivity of spindle organization and length regulation to perturbations at microtubule nucleation sites. This phosphoproteome provides a data set that will guide future work studying the regulation of the SPB and provide insight into the study of individual SPB components.

MATERIALS AND METHODS
Strains, plasmids and media

The yeast strains used in this study were all derived from W303 and are listed in Table 1. C-terminally TAP-tagged proteins were created by PCR amplifying the *TAP-kanMX* cassette from the plasmid TAP-2xPA using primers that shared homology with the flanking sequences of the stop codon in the gene of interest. Cnm67 was N-terminally TAP tagged by PCR amplification of the *TAP-kanMX* cassette from the plasmid PaTEVCa, using primers that shared homology with the flanking DNA of the start codon of *CNM67*. C-terminal mCherry and GFP protein fusions were created by PCR amplification of the *mCherry-hphMX3* and the *GFP-kanMX* cassettes from pBS35 and pFA6-GFP(S65T)::kanMX plasmids, respectively (gifts from the Yeast Resource Center, University of Washington, Seattle, USA). The cassettes for the fluorescent proteins shared homology with the flanking sequence before the stop codon of the genes of interest. For the Cdc20-AID strain, the auxin degron IAA7 was PCR amplified from pSB2065 (gift from Sue Biggins, Fred Hutchinson Cancer Research Center, Seattle, USA) with primers that shared homology with the flanking DNA of the stop codon of the gene. The above cassettes were integrated into a diploid strain, KGY315, and verified by PCR.

The plasmids used in this study are listed in Table 2. QuikChange Lightning Multi Site-Directed Mutagenesis (Stratagene, San Diego, USA)

Table 4. Summary of fluorescent spindle analysis of γ-tubulin small complex phosphorylation mutations

Mutation	Tubulin fluorescence at spindle midzone[B] (compared to WT)	Mean spindle length±s.d.	One tailed P-value of spindle length means (compared to WT)	% Large budded
Wild type (WT)[A]	100%	Spc97: 1.13±0.01 Spc98: 1.06±0.01 Tub4: 1.04±0.01		5.0%
SPC97 S84A	103%	1.21±0.01	0.256	4.0%
SPC97 S84D	101%	1.18±0.01	0.484	7.7%
SPC97 T88A	102%	1.17±0.01	0.002	6.7%
SPC97 T88D	101%	1.17±0.01	0.004	7.7%
SPC97 S84A/T88A	103%	1.22±0.01	<0.00001	10.0%
SPC97 S84D/T88D	98%	1.21±0.01	<0.00001	13.0%
SPC97 S797A	112%	1.15±0.01	0.194	7.0%
SPC97 S797D	106%	1.16±0.01	0.261	9.7%
SPC97 S208A	102%	1.14±0.02	0.450	6.3%
SPC97 S209A	100%	1.8±0.01	0.382	5.7%
SPC98 S152A	100%	1.06±0.01	0.480	5.0%
SPC98 S152D	97%	1.15±0.01	<0.00001	17.3%
TUB4 S71A	98%	1.21±0.02	<0.00001	18.3%
TUB4 S71D	99%	1.05±0.01	0.239	27.7%

[A]WT copies of each gene was integrated in the same strain as the corresponding mutants and used as the WT control for comparisons.
[B]Tubulin fluorescence at the spindle midzone of 1.3–1.6 µm spindles, normalized to the comparable WT strain.

was used to construct plasmids containing point mutations. Plasmids carrying mutations in *SPC97* were integrated at the *SPC97* locus in strain KFY38-5C (*spc97Δ*), plasmids carrying mutations in *SPC98* were integrated at the *SPC98* locus in KFY37-4C (*spc98Δ*), and plasmids carrying mutations in *TUB4* were integrated at the *TUB4* locus in KFY220-1A (*tub4Δ*) using a plasmid shuffle (Widlund and Davis, 2005). These three strains all contained GFP-Tub1 for imaging of microtubules and Spc42-mCherry to visualize spindle pole bodies.

YPD media is as described (Burke et al., 2000). SD-ura low ade and SD-lys were previously described (Sundberg et al., 1996; Tien et al., 2013).

TAP purification and velocity sedimentation

Spindle pole bodies were isolated using a TAP-tag on Spc97, as previously described (Fong et al., 2016). Sucrose gradients were generated by allowing five steps of sucrose solutions (200 µl each of 10%, 20%, 30%, 40%, 2.5 M sucrose) to equilibrate at 4°C for 2 h. For fluorescence analysis, the sucrose solutions were made in 10 mM Bis-Tris, pH 6.5, 0.1 mM MgCl₂. For mass spectrometry analysis, the sucrose solutions were made in 40 mM HEPES, pH 7.4, 150 mM NaCl. The TEV eluate was then applied to the sucrose gradient and spun at 50,000 rpm for 5 h at 4°C in a TLS55 rotor (Beckman Coulter, Brea, USA). SPBs isolated from *cdc4-1* cells were spun at 50,000 rpm for 4 or 4.5 h to prevent side-by-side SPBs from settling to the bottom of the sucrose gradient. Fractions (90 µl) were removed from the top of the gradient with wide-bore tips. The presence of SPBs was determined by western blot analysis, probing for Spc110 (1:2000) and Spc97 (1:3000), using antibodies raised in rabbit and chicken, respectively. Western blot analysis showed the separation of intact SPBs (fractions 9–11) from the soluble pool of SPB components (fractions 1–8).

For isolation of SPBs from cells arrested by depletion of Cdc20, a strain carrying the Cdc20-AID was grown to 80 Klett units in YPD. Auxin (indole-3-acetic acid; IAA) in DMSO was added to a final concentration of 1 mM. Cdc20 was depleted for 1.5 generations before cells were harvested. In Cdc20 depleted cells, ≥98% of cells arrested with large buds. For isolation of SPBs from cells arrested at G1/S, a strain carrying *cdc4-1* was grown at 25°C to 60 Klett units, then shifted to the restrictive temperature of 36°C for two generations before harvesting cells. 95% of cells had elongated buds and 5% had large buds as expected for a *cdc4-1* arrest. Spindle pole bodies were then enriched as previously described (Fong et al., 2016).

Fluorescence microscopy

All images were acquired using a DeltaVision system (Applied Precision, Issaquah, USA) with an IX70 inverted microscope (Olympus, Tokyo, Japan), a U Plan Apo 100× objective (1.35 NA) and a CoolSnap HQ digital

camera (Photometrics, Tuscon, USA). Exposures were 0.4 s for mCherry and GFP. Images were processed as previously described (Shimogawa et al., 2009) using custom Matlab programs (Fluorcal and Calcmate) to identify GFP and mCherry foci and quantify the fluorescence intensities. Fluorcal and Calcmate are available upon request. For live-cell imaging, cells were mounted on an agarose pad as previously described (Muller et al., 2005). Metaphase spindles were identified as spindles with 20–25 pixels (1.3–1.6 µm) between spindle poles. The GFP-tubulin fluorescence intensity distribution was measured and graphed along a normalized spindle length. Fluorescence intensity at the spindle midzone (spindle length of 0.5) was compared to wild-type values. Statistical analysis of spindle length was performed using pairwise z-tests. P-values were computed from pairwise z-scores: $z=(\mu_1-\mu_2)/(\delta_1^2+\delta_2^2)^{0.5}$, where μ_1 and μ_2 are bootstrap average means spindle lengths and δ_1^2 and δ_2^2 are the corresponding standard deviations (Table 4). The budding index of strains was measured by counting 300 cells; large budded cells were defined as those with buds that were two-thirds to equal the size of the mother cell.

For *in vitro* SPB imaging, a flow cell was constructed with KOH cleaned glass coverslips. SPBs were diluted with 5X BRB80/BSA (400 mM K-PIPES, pH 6.9, 5 mM MgCl₂, 5 mM EGTA, 40 mg ml⁻¹ BSA) and KCl to a final concentration of BRB80, 8 mg ml⁻¹ BSA and 500 mM KCl. The diluted SPBs were flowed into the flow cell and allowed to nonspecifically adhere to the coverslip for 30 min before imaging.

Mass spectrometry sample preparation and digestion

Enriched SPB fractions in 40–50% sucrose, 40 mM HEPES, pH 7.4, and 150 mM NaCl, were combined such that samples were approximately 2–30 µg total protein in 0.5 to 1.5 ml of buffer plus approximately 45% sucrose. Samples were diluted 1:1 using 25 mM ammonium bicarbonate (ABC) and concentrated down to 30 µl using Amicon® Ultra 0.5 ml Centrifugal Filters with a 10,000 NMWL (Millipore) according to the manufacturer's instructions. 500 µl of 25 mM ammonium bicarbonate was added to the top of the filter unit and spun through. This was repeated a total of three times. Sample volume was made up to 100 µl of 25 mM ABC and reduced in the filter unit with 10 mM dithiothreitol (DTT) at 37°C for 30 min followed by a 30 min alkylation at room temperature with 15 mM iodoacetamide. 1 µl of 0.8 µg µl⁻¹ Sequencing Grade Modified Trypsin (Promega Corporation, Madison, USA) was used to digest the samples in the filter units at 37°C for 4 h at 1200 rpm in an Eppendorf Thermomixer. After digestion, peptides were spun through the filter units into a new Amicon Eppendorf tube. 100 µl of 25 mM ABC was added to the top of the filter unit and spun through into the same tube. The remaining digested sample was transferred from the filter unit into the Eppendorf tube by pipette. The digested sample was reduced to about 50 µl in a Speedvac.
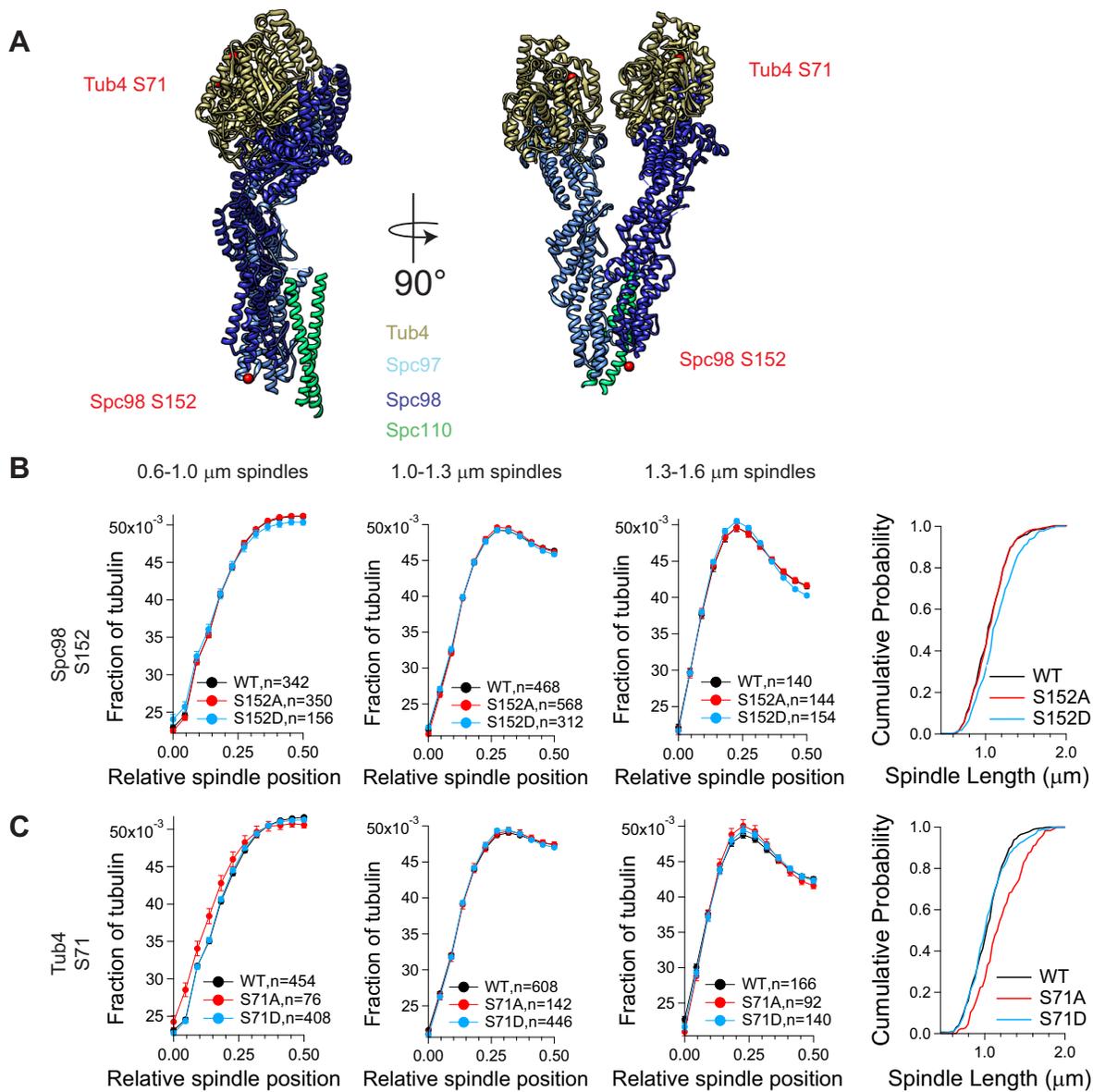
Fig. 4. Phosphorylation regulation of the γ-tubulin small complex is required for normal mitotic spindle morphology. (A) Phosphorylation site S71 is shown on the pseudo-atomic structure of Tub4 (gold) in the yeast γ-tubulin small complex, adapted from PDB:5FM1 (Greenberg et al., 2016). The N-terminal 160 residues of Spc98 are not included in the pseudo-atomic structure, so the exact position of S152 is not shown. (B) Spindle morphology was determined by measuring spindle length and tubulin fluorescence distribution along the spindle. Metaphase spindles were identified as spindles with 1.3–1.6 µm between Spc42-mCherry spindle poles. GFP-Tub1 fluorescence was measured across the entire spindle. (C,D) Half-spindle tubulin distribution profiles for spindles of a given length are shown for Spc98 and Tub4 phosphorylation mutants. Spindle tubulin distributions were separated into two half spindles for ease of display (mean±s.e.m.). In each of the tubulin distribution graphs, the SPB is located at 0 and the spindle equator is located at 0.5. The far right panels show a cumulative probability of spindle length for the observed spindles, measured as the distance between Spc42-mCherry foci. Note that the x-axis begins at 0.45 µm to more clearly display the differences between traces.

Sample pH was adjusted to 2 with 5 M HCl prior to storage at −80°C until mass spectrometry analysis.

Mass spectrometry

Mass spectrometry was performed on either a Q-Exactive or Q-Exactive HF (Thermo Fisher Scientific). 3 µl of sample digest was loaded by autosampler onto a 150-µm Kasil fritted trap packed with Jupiter C12 90 Å material (Phenomenex, Torrance, USA) to a bed length of 2 cm at a flow rate of 2 µl min⁻¹. After loading and desalting using a total volume of 8 µl of 0.1% formic acid plus 2% acetonitrile, the trap was brought online with either a pulled fused-silica capillary tip (75-µm i.d.) or an empty Pico-Frit column (New Objective, Woburn, USA) that was self-packed with 30 cm of

Reprosil-Pur C18-AQ (3-µm bead diameter, Dr Maisch) mounted in an in-house constructed microspray source and placed in line with a Waters Nanoacquity binary UPLC pump plus autosampler. Peptides were eluted off the column using a gradient of 2–35% acetonitrile in 0.1% formic acid over 120 min, followed by 35–60% acetonitrile over 10 min at a flow rate of 250 nl min⁻¹.

The Q-Exactive mass spectrometer was operated using data dependent acquisition (DDA) where a maximum of twenty MS/MS spectra were acquired per MS spectrum (scan range of m/z 400–1600). The resolution for MS and MS/MS was 60,000 and 15,000, respectively, at m/z 200. The automatic gain control (AGC) targets for MS and MS/MS were set to 3e6 and 1e5, respectively, and the maximum fill times were 50 and 25 ms,

respectively. The MS/MS spectra were acquired using an isolation width of 1.6 m/z and a normalized collision energy (NCE) of 27. The underfill ratio was set to 10% and the intensity threshold set to 4e5. MS/MS acquisitions were prevented for unassigned, +1, +6 and greater precursor charge states. Dynamic exclusion (including all isotope peaks) was set for 5 or 10 s. The Q-Exactive HF was operated similarly.

Analysis of mass spectrometry data

Mass spectra from this study and from previously published data were converted into mzML using MSconvert from ProteoWizard (Chambers et al., 2012). With the exception of one asynchronous sample, two technical replicates were run for each biological sample. For each technical replicate, proteins were identified by searching high-resolution MS/MS spectra against the SGD protein sequence database using Comet (Eng et al., 2013). A variable modification of 79.966331 on S, T or Y was included in the search to identify phosphopeptides. Peptide identifications for the two technical replicates were then combined processed with Percolator (Käll et al., 2007). MSDaPl was used to visually inspect the results (Sharma et al., 2012) and confirm there was enough MS2 spectral evidence to differentiate between possible phosphorylated residues in a given peptide and give an accurate assignment. Because data dependent acquisition results in irreproducible sampling collection, additional mass spectrometry runs might reveal more phosphorylation events at each stage of the cell cycle.

Data availability
Analysis of mass spectrometry data can be found at http://www.yeastrc.org/fong_spb_2018. The compiled datasets supporting this article have been uploaded as part of the Supplementary Material.

Supplementary information
Supplementary information available online at
http://bio.biologists.org/lookup/doi/10.1242/bio.033647.supplemental

References

Avena, J. S., Burns, S., Yu, Z., Ebmeier, C. C., Old, W. M., Jaspersen, S. L. and Winey, M. (2014). Licensing of yeast centrosome duplication requires phosphoregulation of Sfi1. *PLoS Genet.* 10, e1004666.

Basto, R. and Pines, J. (2007). The centrosome opens the way to mitosis. *Dev. Cell* 12, 475-477.

Blondel, M., Galan, J. M., Chi, Y., Lafourcade, C., Longaretti, C., Deshaies, R. J. and Peter, M. (2000). Nuclear-specific degradation of Far1 is controlled by the localization of the F-box protein Cdc4. *EMBO J.* 19, 6085-6097.

Bouhlel, I. B., Ohta, M., Mayeux, A., Bordes, N., Dingli, F., Boulanger, J., Velve Casquillas, G., Loew, D., Tran, P. T., Sato, M. et al. (2015). Cell cycle control of spindle pole body duplication and splitting by Sfi1 and Cdc31 in fission yeast. *J. Cell Sci.* 128, 1481-1493.

Bullitt, E., Rout, M. P., Kilmartin, J. V. and Akey, C. W. (1997). The yeast spindle pole body is assembled around a central crystal of Spc42p. *Cell* 89, 1077-1086.

Burke, D. J., Dawson, D. and Stearns, T. (2000). *Methods in Yeast Genetics: A Cold Spring Harbor Laboratory Course Manual*. Cold Spring Harbor, USA: Cold Spring Harbor Laboratory Press.

Burns, S., Avena, J. S., Unruh, J. R., Yu, Z., Smith, S. E., Slaughter, B. D., Winey, M. and Jaspersen, S. L. (2015). Structured illumination with particle averaging reveals novel roles for yeast centrosome components during duplication. *eLife* 4, e08586.

Byers, B. and Goetsch, L. (1974). Duplication of spindle plaques and integration of the yeast cell cycle. *Cold Spring Harb. Symp. Quant. Biol.* 38, 123-131.

Byers, B. and Goetsch, L. (1975). Behavior of spindles and spindle plaques in the cell cycle and conjugation of Saccharomyces cerevisiae. *J. Bacteriol.* 124, 511-523.

Casenghi, M., Barr, F. A. and Nigg, E. A. (2005). Phosphorylation of Nlp by Plk1 negatively regulates its dynein-dynactin-dependent targeting to the centrosome. *J. Cell Sci.* 118, 5101-5108.

Castillo, A. R., Meehl, J. B., Morgan, G., Schutz-Geschwender, A. and Winey, M. (2002). The yeast protein kinase Mps1p is required for assembly of the integral spindle pole body component Spc42p. *J. Cell Biol.* 156, 453-465.

Cha, H., Hancock, C., Dangi, S., Maiguel, D., Carrier, F. and Shapiro, P. (2004). Phosphorylation regulates nucleophosmin targeting to the centrosome during mitosis as detected by cross-reactive phosphorylation-specific MKK1/MKK2 antibodies. *Biochem. J.* 378, 857-865.

Chambers, M. C., Maclean, B., Burke, R., Amodei, D., Ruderman, D. L., Neumann, S., Gatto, L., Fischer, B., Pratt, B., Egertson, J. et al. (2012). A cross-platform toolkit for mass spectrometry and proteomics. *Nat. Biotechnol.* 30, 918-920.

Deshaies, R. J. and Ferrell, J. E. Jr. (2001). Multisite phosphorylation and the countdown to S phase. *Cell* 107, 819-822.

Duncker, B. P., Pasero, P., Braguglia, D., Heun, P., Weinreich, M. and Gasser, S. M. (1999). Cyclin B-Cdk1 kinase stimulates ORC- and Cdc6-independent steps of semiconservative plasmid replication in yeast nuclear extracts. *Mol. Cell. Biol.* 19, 1226-1241.

Eng, J. K., Jahan, T. A. and Hoopmann, M. R. (2013). Comet: an open-source MS/MS sequence database search tool. *Proteomics* 13, 22-24.

Flory, M. R. and Davis, T. N. (2003). The centrosomal proteins pericentrin and kendrin are encoded by alternatively spliced products of one gene. *Genomics* 82, 401-405.

Fong, K. K., Graczyk, B. and Davis, T. N. (2016). Purification of fluorescently labeled saccharomyces cerevisiae spindle pole bodies. *Methods Mol. Biol.* 1413, 189-195.

Friedman, D. B., Sundberg, H. A., Huang, E. Y. and Davis, T. N. (1996). The 110-kD spindle pole body component of Saccharomyces cerevisiae is a phosphoprotein that is modified in a cell cycle-dependent manner. *J. Cell Biol.* 132, 903-914.

Friedman, D. B., Kern, J. W., Huneycutt, B. J., Vinh, D. B. N., Crawford, D. K., Steiner, E., Scheiltz, D., Yates, J., III, Resing, K. A., Ahn, N. G. et al. (2001). Yeast Mps1p phosphorylates the spindle pole component Spc110p in the N-terminal domain. *J. Biol. Chem.* 276, 17958-17967.

Gardner, M. K., Bouck, D. C., Paliulis, L. V., Meehl, J. B., O'Toole, E. T., Haase, J., Soubry, A., Joglekar, A. P., Winey, M., Salmon, E. D. et al. (2008). Chromosome congression by Kinesin-5 motor-mediated disassembly of longer kinetochore microtubules. *Cell* 135, 894-906.

Gartner, A., Jovanović, A., Jeoung, D.-I., Bourlat, S., Cross, F. R. and Ammerer, G. (1998). Pheromone-dependent G1 cell cycle arrest requires Far1 phosphorylation, but may not involve inhibition of Cdc28-Cln2 kinase, in vivo. *Mol. Cell. Biol.* 18, 3681-3691.

Greenberg, C. H., Kollman, J., Zelter, A., Johnson, R., Maccoss, M. J., Davis, T. N., Agard, D. A. and Sali, A. (2016). Structure of γ-tubulin small complex based on a cryo-EM map, chemical cross-links, and a remotely related structure. *J. Struct. Biol.* 194, 303-310.

Huisman, S. M., Smeets, M. F. M. A. and Segal, M. (2007). Phosphorylation of Spc110p by Cdc28p-Clb5p kinase contributes to correct spindle morphogenesis in S. cerevisiae. *J. Cell Sci.* 120, 435-446.

Jaspersen, S. L. and Winey, M. (2004). The budding yeast spindle pole body: structure, duplication, and function. *Annu. Rev. Cell Dev. Biol.* 20, 1-28.

Jaspersen, S. L., Huneycutt, B. J., Giddings, T. H., Resing, K. A., Ahn, N. G. and Winey, M. (2004). Cdc28/Cdk1 regulates spindle pole body duplication through phosphorylation of Spc42 and Mps1. *Dev. Cell* 7, 263-274.

Jeoung, D.-I., Oehlen, L. J. W. M. and Cross, F. R. (1998). Cln3-associated kinase activity in Saccharomyces cerevisiae is regulated by the mating factor pathway. *Mol. Cell. Biol.* 18, 433-441.

Jiang, N., Wang, X., Jhanwar-Uniyal, M., Darzynkiewicz, Z. and Dai, W. (2006). Polo box domain of Plk3 functions as a centrosome localization signal, overexpression of which causes mitotic arrest, cytokinesis defects, and apoptosis. *J. Biol. Chem.* 281, 10577-10582.

Käll, L., Canterbury, J. D., Weston, J., Noble, W. S. and MacCoss, M. J. (2007). Semi-supervised learning for peptide identification from shotgun proteomics datasets. *Nat. Methods* 4, 923-925.

Keck, J. M., Jones, M. H., Wong, C. C. L., Binkley, J., Chen, D., Jaspersen, S. L., Holinger, E. P., Xu, T., Niepel, M., Rout, M. P. et al. (2011). A cell cycle phosphoproteome of the yeast centrosome. *Science* 332, 1557-1561.

Lange, B. M. H. (2002). Integration of the centrosome in cell cycle control, stress response and signal transduction pathways. *Curr. Opin. Cell Biol.* **14**, 35-43.

Lin, T., Gombos, L., Neuner, A., Sebastian, D., Olsen, J. V., Hrle, A., Benda, C. and Schiebel, E. (2011). Phosphorylation of the yeast γ-tubulin Tub4 regulates microtubule function. *PLoS ONE* **6**, e19700.

Lin, T., Neuner, A., Schlosser, Y. T., Scharf, A. N., Weber, L. and Schiebel, E. (2014). Cell-cycle dependent phosphorylation of yeast pericentrin regulates γ-TuSC-mediated microtubule nucleation. *eLife* **3**, e02208.

Muller, E. G. D., Snydsman, B. E., Novik, I., Hailey, D. W., Gestaut, D. R., Niemann, C. A., O'Toole, E. T., Giddings, T. H., Sundin, B. A. and Davis, T. N. (2005). The organization of the core proteins of the yeast spindle pole body. *Mol. Biol. Cell* **16**, 3341-3352.

Niepel, M., Strambio-de-Castillia, C., Fasolo, J., Chait, B. T. and Rout, M. P. (2005). The nuclear pore complex-associated protein, Mlp2p, binds to the yeast spindle pole body and promotes its efficient assembly. *J. Cell Biol.* **170**, 225-235.

Oakley, B. R., Oakley, C. E., Yoon, Y. and Jung, M. K. (1990). γ-tubulin is a component of the spindle pole body that is essential for microtubule function in Aspergillus nidulans. *Cell* **61**, 1289-1301.

O'Toole, E. T., Winey, M. and McIntosh, J. R. (1999). High-voltage electron tomography of spindle pole bodies and early mitotic spindles in the yeast Saccharomyces cerevisiae. *Mol. Biol. Cell* **10**, 2017-2031.

Peng, Y., Moritz, M., Han, X., Giddings, T. H., Lyon, A., Kollman, J., Winey, M., Yates, J., Agard, D. A., Drubin, D. G. et al. (2015). Interaction of CK1δ with γTuSC ensures proper microtubule assembly and spindle positioning. *Mol. Biol. Cell* **26**, 2505-2518.

Pereira, G., Knop, M. and Schiebel, E. (1998). Spc98p directs the yeast γ-tubulin complex into the nucleus and is subject to cell cycle-dependent phosphorylation on the nuclear side of the spindle pole body. *Mol. Biol. Cell* **9**, 775-793.

Peter, M. and Herskowitz, I. (1994). Direct inhibition of the yeast cyclin-dependent kinase Cdc28-Cln by Far1. *Science* **265**, 1228-1231.

Rieder, C. L., Faruki, S. and Khodjakov, A. (2001). The centrosome in vertebrates: more than a microtubule-organizing center. *Trends Cell Biol.* **11**, 413-419.

Sharma, V., Eng, J. K., Maccoss, M. J. and Riffle, M. (2012). A mass spectrometry proteomics data management platform. *Mol. Cell. Proteomics* **11**, 824-831.

Shimogawa, M. M., Widlund, P. O., Riffle, M., Ess, M. and Davis, T. N. (2009). Bir1 is required for the tension checkpoint. *Mol. Biol. Cell* **20**, 915-923.

Sikorski, R. S. and Hieter, P. (1989). A system of shuttle vectors and yeast host strains designed for efficient manipulation of DNA in Saccharomyces cerevisiae. *Genetics* **122**, 19-27.

Stearns, T., Evans, L. and Kirschner, M. (1991). γ-tubulin is a highly conserved component of the centrosome. *Cell* **65**, 825-836.

Stirling, D. A. and Stark, M. J. R. (1996). The phosphorylation state of the 110 kDa component of the yeast spindle pole body shows cell cycle dependent regulation. *Biochem. Biophys. Res. Commun.* **222**, 236-242.

Sundberg, H. A., Goetsch, L., Byers, B. and Davis, T. N. (1996). Role of calmodulin and Spc110p interaction in the proper assembly of spindle pole body components. *J. Cell Biol.* **133**, 111-124.

Tien, J. F., Fong, K. K., Umbreit, N. T., Payen, C., Zelter, A., Asbury, C. L., Dunham, M. J. and Davis, T. N. (2013). Coupling unbiased mutagenesis to high-throughput DNA sequencing uncovers functional domains in the Ndc80 kinetochore protein of Saccharomyces cerevisiae. *Genetics* **195**, 159-170.

Viswanath, S., Bonomi, M., Kim, S. J., Klenchin, V. A., Taylor, K. C., Yabut, K. C., Umbreit, N. T., Van Epps, H. A., Meehl, J., Jones, M. H. et al. (2017). The molecular architecture of the yeast spindle pole body core determined by Bayesian integrative modeling. *Mol. Biol. Cell* **28**, 3298-3314.

Vogel, J., Drapkin, B., Oomen, J., Beach, D., Bloom, K. and Snyder, M. (2001). Phosphorylation of γ-tubulin regulates microtubule organization in budding yeast. *Dev. Cell* **1**, 621-631.

Widlund, P. O. and Davis, T. N. (2005). A high-efficiency method to replace essential genes with mutant alleles in yeast. *Yeast* **22**, 769-774.

Winey, M. and Bloom, K. (2012). Mitotic spindle form and function. *Genetics* **190**, 1197-1224.

Winey, M., Goetsch, L., Baum, P. and Byers, B. (1991). MPS1 and MPS2: novel yeast genes defining distinct steps of spindle pole body duplication. *J. Cell Biol.* **114**, 745-754.

Woodruff, J. B., Wueseke, O. and Hyman, A. A. (2014). Pericentriolar material structure and dynamics. *Philos. Trans. R. Soc. Lond. B Biol. Sci.* **369**, 20130459.

Woodruff, J. B., Wueseke, O., Viscardi, V., Mahamid, J., Ochoa, S. D., Bunkenborg, J., Widlund, P. O., Pozniakovsky, A., Zanin, E., Bahmanyar, S. et al. (2015). Centrosomes. Regulated assembly of a supramolecular centrosome scaffold in vitro. *Science* **348**, 808-812.